Sequential Hydrogen Tunneling in *o*-Tolylmethylene

Thomas Lohmiller[+],[c, d] Sujan K. Sarkar[+],[a, e] Jörg Tatchen,[b] Stefan Henkel,[a, f] Tim Schleif,[a] Anton Savitsky,[c, g] Elsa Sanchez-Garcia,*[b] and Wolfram Sander*[a]

In memoriam Klaus Hafner

Abstract: *o*-Tolylmethylene **1** is a metastable triplet carbene that rearranges to *o*-xylylene **2** even at temperatures as low as 2.7 K via [1,4] H atom tunneling. Electron paramagnetic resonance (EPR) and electron nuclear double resonance (ENDOR) spectroscopical techniques were used to identify two conformers of **1** (*anti* and *syn*) in noble gas matrices and in frozen organic solutions. Conformer-specific kinetic measurements revealed that the rate constants for the rearrangements of the *anti* and *syn* conformers of **1** are very similar. However, the orbital alignment in the *syn* conformer is less favorable for the hydrogen transfer reaction than the orbital configuration in the *anti* conformer. Our spectroscopic and quantum chemical investigations indicate that *anti* **1** and *syn* **1** rapidly interconvert via efficient quantum tunneling forming a rotational pre-equilibrium. The subsequent second tunneling reaction, the [1,4] H migration from *anti* **1** to **2**, is rate-limiting for the formation of **2**. We here present an efficient strategy for the study of such tunneling equilibria.

Introduction

Quantum mechanical tunneling (QMT) has long been recognized as a general phenomenon in chemistry,[1] providing an alternative mode of reaction to the classical thermal pathway. Due to its great mass-dependency, QMT is most pronounced in reactions involving the transfer of a hydrogen atom, with numerous examples of hydrogen tunneling reported in the literature.[2] Matrix isolation is a tool of choice to study such reactions, since cryogenic temperatures suppress competing thermal reaction pathways. An early example of a [1,4] hydrogen shift observed by matrix isolation spectroscopy is the rearrangement of triplet *o*-tolylmethylene **1** to *o*-xylylene **2** reported by McMahon and Chapman (Scheme 1).[3] By using electron paramagnetic resonance (EPR) and UV-vis spectroscopy, the reaction kinetics was determined, and temperature-independent rate constants in the order of $10^{-6}\,s^{-1}$ were found.

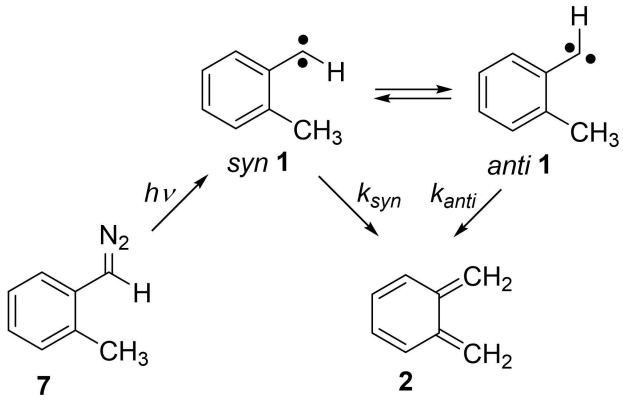

Scheme 1. Conformer-specific hydrogen tunneling in triplet *o*-tolylmethylene **1**.[3b]

[a] Dr. S. K. Sarkar,[+] Dr. S. Henkel, Dr. T. Schleif, Prof. W. Sander
Lehrstuhl für Organische Chemie II,
Ruhr-Universität Bochum
44780 Bochum (Germany)
E-mail: wolfram.sander@ruhr-uni-bochum.de

[b] Dr. J. Tatchen, Prof. E. Sanchez-Garcia
Computational Biochemistry,
Universität Duisburg-Essen
45141 Essen (Germany)
E-mail: elsa.sanchez-garcia@uni-due.de

[c] Dr. T. Lohmiller,[+] Dr. A. Savitsky
Max-Planck-Institut für Chemische Energiekonversion
45470 Mülheim an der Ruhr (Germany)

[d] Dr. T. Lohmiller[+]
EPR4Energy Joint Lab,
Abteilung Spins in der Energieumwandlung und Quanteninformatik
Helmholtz-Zentrum Berlin für Materialien und Energie GmbH
12489 Berlin (Germany)

[e] Dr. S. K. Sarkar[+]
present address: The University of Hong Kong
Hong Kong SAR (China)

[f] Dr. S. Henkel
present address: Lehrstuhl für Physikalische Chemie II
Ruhr-Universität Bochum
44780 Bochum (Germany)

[g] Dr. A. Savitsky
present address: Experimentelle Physik 3
Technische Universität Dortmund,
44221 Dortmund (Germany)

[+] These authors contributed equally to this work.

Supporting information for this article is available on the WWW under https://doi.org/10.1002/chem.202102010

Temperature-independent reaction rates are characteristic for QMT.[3b] For this reaction, McMahon and Chapman stated that *"the major rotomer decays much more rapidly than the minor rotomer"* since it has a *"more appropriate geometry for hydrogen migration"*.[3] However, a detailed analysis of the difference in kinetic behaviour of the two conformers was not reported.

Recent studies renewed the interest in conformational control[4] of tunneling reactions as exemplified by the investigations of the [1,2]-hydrogen shift in hydroxycarbenes **3**.[5] For the hydrogen shift in hydroxycarbenes **3** or the ring expansion in fluorocarbene **5**[6] to proceed (Scheme 2), the respective carbene center has to be correctly aligned with respect to the adjacent proton (for **3**) or carbon atom (for **5**). This is necessary to minimize the structural rearrangement required to produce the corresponding products **4** or **6**, respectively. In both cases, no interconversion between the respective conformers via thermal reaction or tunnelling was detected. In addition, the tunnelling processes were observed to be highly conformer-specific, with only the suitably aligned conformer being able to undergo facile rearrangement.

Here we report the assignment of the *syn* and *anti* conformers of **1** based on EPR and electron nuclear double resonance (ENDOR) spectroscopies in frozen solution and solid noble gas matrices. Furthermore, we explore the conformer specificity of the **1**→**2** rearrangement at 5–10 K, aided by small curvature tunnelling (SCT) calculations. Our findings reveal a consistent reaction sequence including tunneling between *syn* and *anti*, constituting a pre-equilibrium, and rate-limiting [1,4] H migration from *anti* **1** to **2**.

Results and Discussion

EPR and ENDOR spectroscopy

UV irradiation of *o*-tolyldiazomethane **7** in an argon matrix results in an X-band continuous wave (CW) EPR spectrum that contains a dominant set of characteristic triplet signals at magnetic field positions of 196, 495, 598 and 878 mT (Figure 1, top). A smaller triplet contribution with slightly different zero field splitting (zfs) parameters is observed at 501 and 592 mT, though partially overlapping with the signals of the major component. Based on the x_{+1} signal, the ratio of the two triplet species is estimated to be about 90:10. The zfs parameters from spectral simulations are in agreement with those reported in literature (Table 1).[3b] Calculations of the two rotamers of **1** place the *syn* conformer, in which the carbene hydrogen atom is pointing towards the methyl group (Scheme 1), 0.3 kcal mol^{-1}

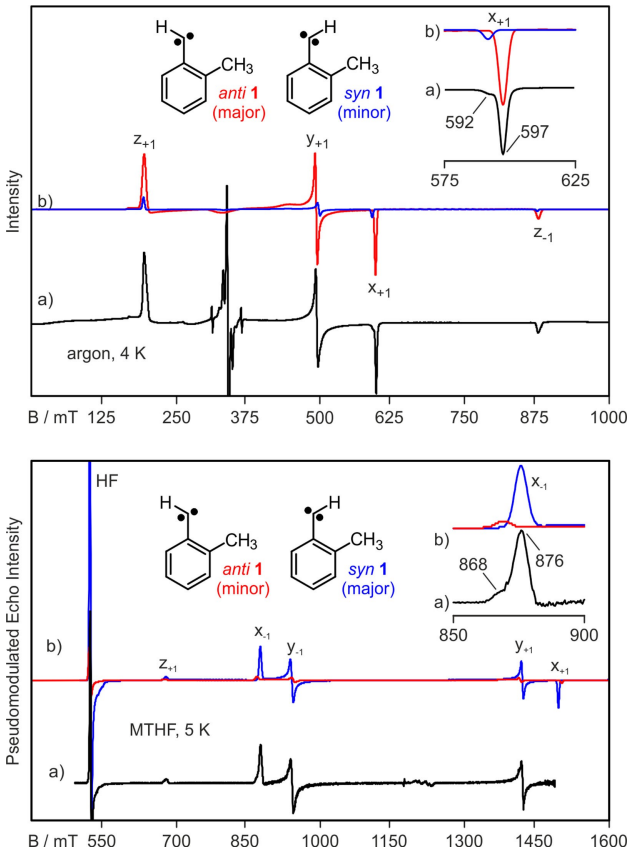

Figure 1. EPR spectra of **1** in different cryogenic environments. *Top.* a) X-band CW EPR spectrum of **1** in argon at 4 K ($\nu = 9.578$ GHz). b) Simulated triplet spectra with D(major) = 0.5063 cm^{-1}, $|E$(major)$|$ = 0251 cm^{-1} and D(minor) = 0.505 cm^{-1}, $|E$(minor)$|$ = 0.0226 cm^{-1}. *Bottom.* a) Pseudo-modulated Q-band pulse EPR spectrum of **1** in MTHF at 5 K ($\nu = 34.03$ GHz). b) Simulated triplet spectra with D(major) = 0.5003 cm^{-1}, $|E$(major)$|$ = 0.0217 cm^{-1} and D(minor) = 0.5029 cm^{-1}, $|E$(minor)$|$ = 0.0249 cm^{-1}. Insets show the most distinct spectroscopic features of the two triplet components: x_{+1} at X-band (outside the maximum B field at Q-band) and x_{-1} at Q-band (not resolved at X-band). As the transitions relate to different sublevels, the relative positions of *anti*/*syn* **1** are inverted. For the nomenclature of the transitions, see Supporting Information section S2.

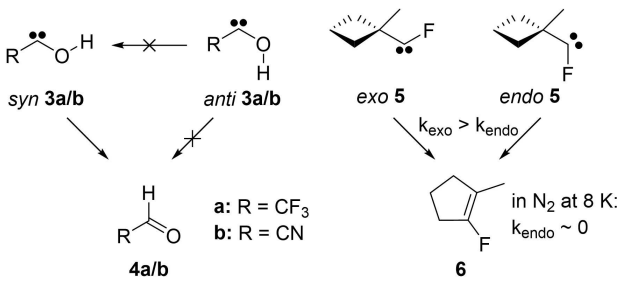

Scheme 2. Examples of conformer-specific hydrogen or carbon tunneling in carbenes: singlet hydroxycarbenes **3 a/b**[5] and singlet fluorocarbene **5**, respectively.[6]

Table 1. Zero-field splitting parameters of *syn* **1** and *anti* **1**. Values shown in bold are those of the major components.

	anti **1** D/cm^{-1}	$\|E\|$/cm^{-1}	*syn* **1** D/cm^{-1}	$\|E\|$/cm^{-1}
Ar/4 K[a]	**0.5063**	**0.0251**	0.5050	0.0226
Ar/20 K[3b]	**0.503**	**0.0253**	0.503	0.0244
MTHF/5 K[a]	0.5029	0.0249	**0.5003**	**0.0217**
calc.[b]	**0.4861**	**0.0249**	0.4811	0.0223

[a] Based on linewidths and total spectral widths, relative errors of the fitted zfs parameters are estimated to be significantly below 1%. [b] TPSSh-D3/def2-TZVP level of theory, E values are predicted to be negative.

above the *anti* conformer (BLYP-D3/6-311G** level of theory, *in vacuo*). Thus, the major component observed in the matrix EPR spectrum is expected to be *anti* **1**. This assignment is supported by calculated zfs parameters yielding different *D* and *E* values for the two conformers of **1**, with larger values for the *syn* conformer (Table 1, $\Delta D \approx 1\%$, $\Delta E \approx 10\%$).

A similar set of triplet signals is observed in a Q-band pulse EPR spectrum obtained upon photolysis of precursor **7** in frozen 2-methyltetrahydrofuran (MTHF). It contains 5 lines with higher intensity at 524, 679, 876, 942 and 1421 mT and a second, weaker set of signals, best identified by the distinct features at the x_{-1} position, shifted to 868 mT (Figure 1, bottom). Comparison with the spectrum obtained in solid argon reveals that the intensity ratio of the two triplet species is inverted in MTHF with a ratio of approximately 15:85 in favor of the species with smaller simulated zfs splitting parameters, which is assigned to the *syn* conformer of **1** (Table 1, Figure S4). Accordingly, the behavior of **1** differs significantly depending on whether the molecules are prepared in a condensed noble gas matrix or a frozen organic glass with respect to the ratio of the two conformers. This can be related to either steric restrictions of the conformational isomerization of the nascent carbene, as the precursor **7** is found exclusively in the 1-H *syn* conformation (see below), or to stabilization of *syn* **1** by interactions with the frozen solvent. The ratio of the two components in MTHF was found to be virtually unaffected by increasing the temperature from 5 to 10 K (Figure S1) or by changing the solvent to toluene-d_8 (not shown), indicating that in the frozen organic solvents, even more than in the noble gas matrix, reaching the thermodynamic equilibrium is kinetically hindered.

However, a definite assignment of the two conformers in the different environments cannot be made based solely on the comparison with theoretical zfs parameters from *in vacuo* DFT, especially considering the small difference in *D* values and the similar energies predicted for the two conformers. Therefore, ENDOR spectroscopy was employed to investigate the spatial and electronic structures of **1**. The ^{1}H electron-nuclear hyperfine interactions provide insight into the spin density distribution across the molecule and thus allow to characterize the conformational distribution of a carbene molecule, as we recently demonstrated.[7]

Figure 2 shows the Q-band Davies-type ^{1}H-ENDOR spectrum of **1** in MTHF recorded at the z_{+1} magnetic field position of the major component in the EPR spectrum, together with spin-Hamiltonian-based simulations for the two conformers employing the theoretical EPR parameters from the DFT computations (Table S1). The spectra at the x_{-1} and y_{-1} positions are shown in Figure S2. Considering that DFT calculations tend to slightly overestimate the magnitude of ^{1}H hyperfine couplings in triplet carbenes,[7] the major peaks in the experimental ENDOR spectrum in MTHF are assigned to the *syn* conformer of **1**. This becomes particularly evident for the spectrum recorded at the z_{+1} position, which exclusively comprises a single molecular orientation. While the simulated spectral width of *syn* **1** agrees well with the experiment, the calculated position of +13.4 MHz for H_4 in *anti* **1** lies clearly above the highest experimental resonance frequency of +8.2 MHz. Thus, the major component

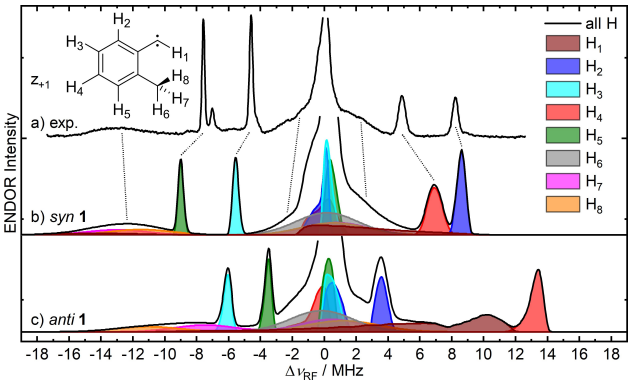

Figure 2. Q-band Davies-type ^{1}H-ENDOR. a) Experimental spectrum of **1** in MTHF at the z_{+1} field position of the major spectral contribution of the corresponding EPR spectrum (Figure 1). b), c) Simulations for *syn* **1** and *anti* **1**, respectively, employing the ***g***, ***d*** and ***a*** matrices calculated at the TPSSh-D3/def2-TZVP level of theory (Table S1). Spectra at the x_{-1} and y_{-1} positions are shown in Figure S2.

in MTHF can be unambiguously assigned to the *syn* conformer, while the minor component represents the *anti* conformer, in agreement with the assignment based on calculated zfs values.

IR spectroscopy

Next, we re-investigated the conformers *syn* **1** and *anti* **1** by IR spectroscopy. The spectroscopic features of the diazo precursor **7** isolated in an argon matrix can be reproduced by assuming the presence of only the less sterically congested conformer *syn* **7** (see Supporting Information). This assumption is consistent with the predicted relative stability of *syn* **7** (1.9 kcal mol^{-1} at the BLYP-D3/6-311G** level of theory). In agreement with the literature,[3b] irradiation of *syn* **7** with $\lambda = 254$ nm results in the formation of carbene **1** as well as secondary photolysis yielding *o*-xylylene **2**. Despite some splitting of the characteristic peaks of the carbene, it was not possible to unambiguously assign IR signals to the individual rotamers of carbene **1**.

In the dark, **1** slowly rearranges to **2**, and from the spectroscopic changes in the IR spectrum, rates in the order of $2.1 \cdot 10^{-5}$ s^{-1} were determined in argon and xenon at 3 K (Table 2). These values are in agreement with previously reported data, which was re-evaluated using the same kinetic model.[3b] The lack of deconvolution of the experimental IR spectrum with respect to the contribution of the two conformers *syn* **1** and *anti* **1** limits any kinetic information via IR (or UV) spectroscopy to an average rate constant. Thus, if there is a difference in rates for the two conformers of **1**, the analysis will only yield the faster contribution.

EPR Kinetics

A kinetic analysis was carried out for the EPR time dependencies at magnetic field positions specific for either *syn* or *anti* **1** (Table 2). McMahon and Chapman reported that "*the major*

Table 2. Rate constants for the rearrangement (d_1-/d_3-)*syn*/*anti* **1**→**2**.

matrix/solvent	rate constants/10^{-5} s^{-1}					
	syn **1**	*anti* **1**	*syn* d_1-**1**	*anti* d_1-**1**	*syn* d_3-**1**	*anti* d_3-**1**
Ar (5 K, UV)[a]	1.4 ± 1.1		[e]		[g]	
Ar (3 K, IR)[b]	2.1 ± 0.1 (3.1 ± 0.1)[f]		2.1 ± 0.1 (2.9 ± 0.1)[f]		[g]	
Xe (3 K, IR)[b]	2.3 ± 0.1		2.1 ± 0.2		[e]	
Ar (4 K, EPR)[c]	2.1 ± 0.6	1.9 ± 0.3	[e]	[e]	[g]	[g]
MTHF (5 K, EPR)[d]	0.9 ± 0.1	1.2 ± 0.0	[e]	[e]	[g]	[g]
MTHF (10 K, EPR)[d]	2.3 ± 0.7	1.3 ± 0.2	[e]	[e]	[e]	[e]

[a] From re-evaluation of the UV intensity around 249 nm (**1**) reported by McMahon and Chapman.[3b] [b] From fits of the time dependence of the IR intensity around 741–743 cm^{-1} (**1**), 773–776 cm^{-1} (**2**) and 864–872 cm^{-1} (**2**), slightly adjusted for deuterated species or experiments in xenon matrices. [c] From fits of the time dependence of the CW EPR intensity around 592 mT (*syn* **1**) and 597 mT (*anti* **1**), deconvoluted by fitting two Voigt profiles. [d] From fits of the time-dependence of the pseudomodulated pulse EPR intensity around 866 mT (*syn* **1**) and 875–876 mT (*anti* **1**). [e] Not reported/not determined. [f] From experiments using a broadband pass filter with a cutoff > 1500 cm^{-1}. [g] No reaction observed.

rotomer decays much more rapidly than the minor rotomer".[3b] Indeed, a comparison of EPR spectra in argon recorded at the beginning of the kinetic measurement and after several hours show a clear decrease in the intensity ratio *anti*/*syn* (Figure 3, top). However, rates of about $2.0 \cdot 10^{-5}\,s^{-1}$, consistent with the result from the IR measurements, are obtained for *both* isomers. The apparent difference in their spectral decays is instead caused by different ratios *c* [Eq. (1)] of non-reactive residuals of the two isomers (Ar, 4 K; *syn* **1**: 0.73, *anti* **1**: 0.11), which represent the lower limits at which the decay curves saturate. This can be deduced from the decrease in the relative intensities: For the dominant *anti* isomer, the intensity decreases to a limiting value of roughly 30%, while at the same time the *syn* isomer approaches 80%, despite nearly identical reaction rates.

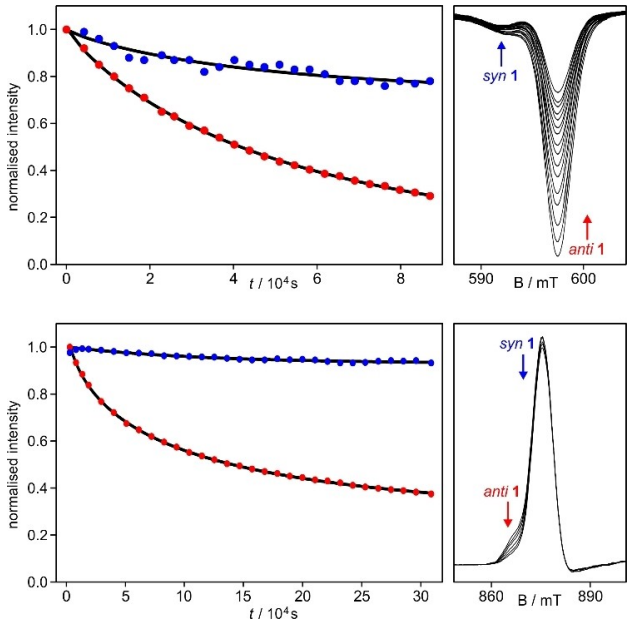

Figure 3. Kinetic analysis of the tunneling rearrangement. *Top*: Decrease in normalized intensities of the X-band EPR x_{+1} signals attributed to *syn* and *anti* **1** in argon at 4 K. *Bottom*: Decrease in normalized intensities of the Q-band EPR x_{-1} signals attributed to *syn* and *anti* **1** in MTHF at 5 K (compare Figure 1). The black lines show the best fit results obtained using the kinetic model [Eq. (1) in the Experimental Section].

The reaction rate of the **1**→**2** reaction in frozen MTHF matrices at 5 K is roughly half of those found in argon (Figure 3, bottom, Table 2), with decay curves leveling off to 37% (*anti* **1**) and 93% (*syn* **1**). At elevated temperatures of 10 K, the decay rates are moderately increased for the *syn* isomer, but virtually unaltered for the *anti* isomer. This increase can be attributed to temperature-dependent side reactions with the organic matrix material, to which the reactive carbene site is more exposed in *syn* **1**.

A large primary kinetic isotope effect has been reported for CD_3-substituted **1**,[3b] i.e., deuteration of the methyl group suppresses the tunneling rearrangement to d_3-**2**. This behavior was also found in our experiments. Furthermore, the EPR spectra of d_3-**1** do not show a change in the isomer ratio over time (Figure S3) and thus no unidirectional *syn*→*anti* interconversion. Additionally, d_1-**1** with the deuterium attached to the carbene carbon atom was investigated to study the influence of the *syn*/*anti* interconversion on the **1**→**2** tunneling rate. Based on IR measurements, identical rates were found for d_1-**1**, indicating that there is no pronounced secondary kinetic isotope effect.

The presence of unreactive or trapped fractions within the ensemble is not uncommon for molecules isolated at cryogenic temperatures.[8] As already indicated by the differing *anti*/*syn* **1** ratio in noble gas and organic matrices, steric restrictions resulting from interactions with the non-uniform molecular environment kinetically impede processes towards the thermodynamic minimum. Apparently, this is the case for both the isomerization from *syn* **1** to *anti* **1** upon photolysis of **7**, the *syn* conformation of 1-H being the energetic minimum of **7** (see Supporting Information section S8), as well as for the [1,4] H shift, as indicated by the unreactive residuals of *anti* **1** ($c > 0$). Steric hindrance removes part of the ensemble from the *anti*/*syn* **1** equilibrium, resulting in differing residuals c(*syn* **1**) > c(*anti* **1**). Restrained or frozen sites could be blocked both by the matrix or solvent, as well as by N_2 molecules partially still occupying the position close to the divalent carbon after photolysis. These effects are more pronounced in organic glasses, which can be rationalized by stronger interactions with the solute and higher matrix rigidity as compared to the noble gas matrices, and lower mobility of residual N_2.

Computational studies

Geometrically, the transfer of a hydrogen atom from the methyl group to the carbene center is not feasible for *syn* **1** and therefore tunneling to **2** is expected to take place exclusively from *anti* **1**. The decrease of *syn* **1** is therefore attributed to a (tunneling) conversion to the *anti* isomer, which in turn can react to **2**. Since no *syn*→*anti* interconversion is observed for

the d_3-isotopologue, it is hypothesized that the two isomers are in equilibrium. A fast (tunneling) *anti/syn* **1** pre-equilibrium yields identical disappearance rates for the two isomers reflecting the conversion of *anti* **1** to **2**.

For *anti* **1**, rotation of the methyl group by 60° from its minimum position will decrease the tunneling distance and thus increase the tunneling probability (Figure 4). In our calculations, this displacement is described by a valley-ridge inflection (VRI) point, corresponding to the transition state (TS) of the methyl group rotation, connected to the TS of the hydrogen transfer reaction. Experimentally, however, it is not possible to discriminate whether tunneling takes place from the minimum structure of *anti* **1**, from the geometry with optimal CH_3 rotation (i.e. the VRI point) or from an intermediary state. The primary product obtained from the rearrangement of **1** in its triplet ground state will be triplet T-**2**. Here too, the geometry to which an in-plane hydrogen transfer is leading corresponds to a VRI point, in which one of the methylene groups of **2** is rotated by 90° from its minimum position. Subsequent rotation and intersystem crossing will lead to the final product, xylylene **2**.

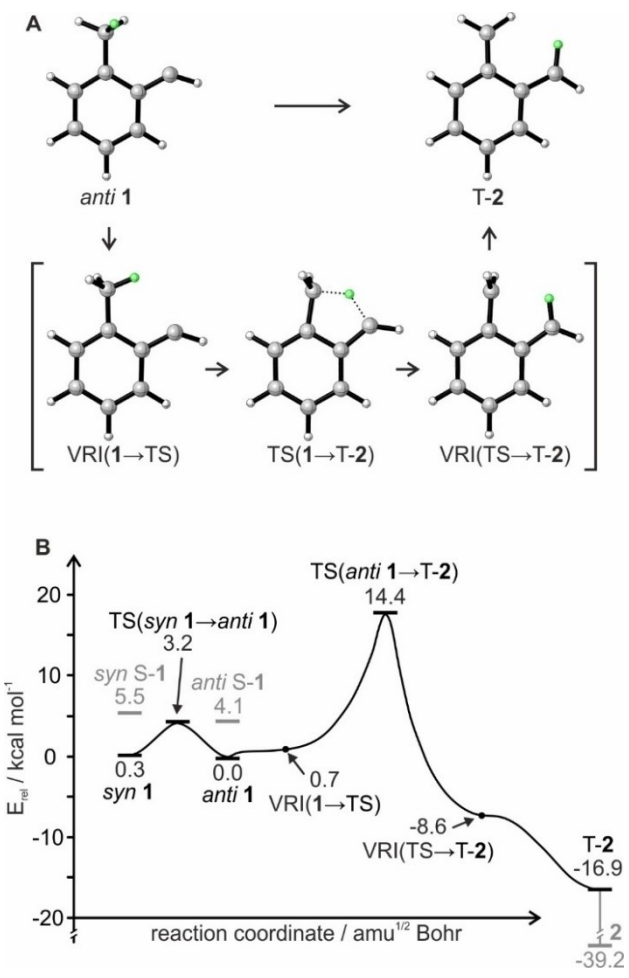

Figure 4. A) Calculated geometries for the tunneling rearrangement of **1**. B) Potential energy surface of the *syn*/*anti* isomerization of **1** and subsequent rearrangement to **2**. Energy values include zero-point vibrational energies. All calculations were performed at the BLYP-D3/6-311G** level of theory.

Tunneling rates were calculated with the SCT method for the elementary reaction steps of the **1**→T-**2** tunneling reaction (Table 3). The tunneling rate of the *syn* **1**→*anti* **1** isomerization is predicted to a remarkably large value of $3.6 \cdot 10^7\ s^{-1}$. Such highly efficient tunneling close to zero Kelvin is attributed to the light weight of the tunneling atom, as the tunneling coordinate is dominated by the movement of the methylene hydrogen atom and a low barrier height of 2.9 kcal mol^{-1}. Thus, the isomerization is mostly occurring by tunneling at temperatures of 100 K and below, while classical barrier passage is predicted to contribute approximately half of the overall reaction turnover at room temperature. Deuteration at the carbene position (d_1-**1**) induces a strong kinetic isotope effect (KIE) and slows down this rate by approximately a factor of 36. However, the resulting rate constant is still predicted to be too fast to be detected experimentally. A slight inverse secondary KIE is found for d_3-**1**.

Tunneling rates were also calculated for the *anti*→*syn* **1** isomerization, which is endothermic. Hence, tunneling from the *anti* conformer towards the more energetic *syn* conformer is only possible via vibrational excitation, and the SCT rate *k*(*syn*→*anti* **1**) will outperform *k*(*anti*→*syn* **1**) at very low temperatures. Accordingly, *k*(*anti*→*syn* **1**) exhibits a substantial rise by 3–4 orders of magnitude upon approaching 20 K, not found for *k*(*syn*→*anti* **1**) (see Supporting Information).

The rates of the [1,4] H migration were calculated only for *anti* **1** due to the lack of a reasonable transition structure for a direct *syn* **1**→T-**2** reaction. The rate *k*(*anti* **1**→T-**2**) predicted at 20 K is $2.4 \cdot 10^{-2}\ s^{-1}$, which deviates from the experimental value in Ar at 3 K by roughly three orders of magnitude. Graphical extrapolation of the calculated rates to estimate the values below 20 K does not bring them into agreement. The discrepancy between experimental and computed rates is most likely a limitation of the method, which does not describe the reaction barrier accurately enough and which does not include solvent effects.

At temperatures below 100 K, the [1,4] H migration is predicted to occur exclusively due to tunneling (Figure 5). However, even at 300 K, tunneling still represents the main contribution to the overall turnover. Consistent with the experiment, a small secondary KIE is found for d_1-**1**, while a large KIE of five orders of magnitude is found upon deuteration of the methyl group, effectively suppressing the rearrangement in d_3-**1**.

Table 3. SCT rate constants at 20 K for the **1**→T-**2** reaction steps at the BLYP-D3/6-311G** level of theory.

	calculated rate constants k/s^{-1}		
	1	d_1-**1**	d_3-**1**
syn→anti **1**	$3.6 \cdot 10^7$	$1.0 \cdot 10^6$	$4.4 \cdot 10^7$
anti→syn **1**	$9.7 \cdot 10^3$	$3.1 \cdot 10^2$	$1.8 \cdot 10^4$
anti **1**→T-**2**	$2.4 \cdot 10^{-2}$	$9.3 \cdot 10^{-3}$	$5.2 \cdot 10^{-7}$
1→**2** (exp)	$2.1 \cdot 10^{-5}$	$2.1 \cdot 10^{-5}$	not observed

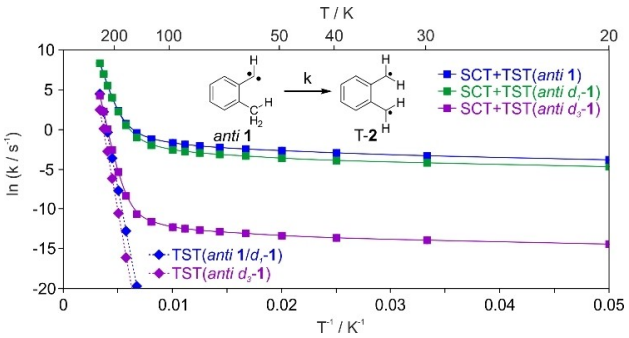

Figure 5. Reaction rates calculated via transition state theory (TST) only and including tunneling (SCT) corrections at the BLYP-D3/6-311G** level of theory for the (d_1/d_3-)*anti* **1**→T-**2** reaction.

Conclusion

The conformational isomerism and hydrogen tunneling of triplet *o*-tolylcarbene **1**, previously reported by McMahon and Chapman,[3] were re-investigated by us using advanced spectroscopic and quantum chemical techniques. ENDOR spectroscopy provides a reliable method to identify the two conformers, which in turn allowed us to confidently assign the conformers of **1** in the EPR spectra as required for the conformer-specific kinetic experiments.

Tunneling rates are highly dependent on the tunneling distance. To enable rapid [1,4] H tunneling in **1**, it is therefore crucial that the carbene adopts a proper conformation with a short distance between the migrating H atom and the carbene center. To achieve this, the carbene must adopt its *anti* conformation and the methyl group has to rotate from its minimum conformation by 60° to structure VRI(**1**→TS) (Figure 4). Nevertheless, our EPR studies reveal the same tunneling rates for both *syn* and *anti* **1**. This observation is in notable contrast to the large differences in tunneling rates found for the conformers of singlet hydroxy- or fluorocarbenes.[5a,6]

We conclude that the (non-confined fractions of the) *syn* and *anti* conformers are in rapid equilibrium even at temperatures between 3 and 5 K. The classical activation barrier is calculated to 2.9 kcal/mol, which should completely suppress this rearrangement at temperatures below 5 K. This clearly indicates that the *syn*→*anti* rearrangement is governed by tunneling, in agreement with the predictions from our SCT calculations. Even after deuterium substitution of the hydrogen atom at the carbene center, the decrease of the tunneling rate is not sufficient to become rate determining for the overall process. The hydrogen migration in the *syn* conformer therefore requires a sequential tunneling reaction: first *syn*→*anti* isomerization and second [1,4] H migration. If we assume that the CH_3 rotation is also governed by tunneling, we must consider three consecutive tunneling movements required for the **1**→**2** rearrangement. Thus, in contrast to the reactions in singlet hydroxy- or fluorocarbenes,[5a,6] **1** exhibits conformer-specific hydrogen tunneling to which the Curtin-Hammett principle[9] applies. This describes a situation where the (tunneling) barrier for conformer interconversion is considerably lower than that of the actual reaction under consideration. For **1**, it allows for a rotational tunneling pre-equlibrium to exist, which in turn disguises the conformer-specificity of the [1,4] H migration.

Tunneling reactions play a vital role in chemistry and biology, particularly in C–H activation reactions.[2b,d, e] Conformational pre-equilibria are important to achieve geometries with high tunneling probabilities,[10] therefore our observation of sequential tunneling will aid in the fundamental understanding of such complex reaction sequences.

Experimental Section

Experimental details

Matrix isolation experiments were performed using standard techniques.[11] The diazo precursor **7** was prepared by thermolysis of the corresponding sodium tosyl hydrazonide at 50 °C, immediately sublimed into vacuum and deposited with a large excess of argon on top of a CsI disk or a copper rod cooled to temperatures of 4 K by a closed-cycle helium cryostat, to record matrix-isolation IR and X-band CW EPR spectra, respectively. Photolysis was carried out with 254 nm low-pressure mercury lamp. Q-band pulse EPR and ENDOR experiments were performed at 5 K or 10 K using a Bruker ELEXSYS E580 spectrometer equipped with a homebuilt TE_{011} microwave cavity,[12] a cryogen-free closed-cycle cryostat (Cryogenic Ltd.) and an ENI 3200 L radio frequency (RF) amplifier. For further details about pulse-sequences, spectral simulations and DFT calculations of EPR parameters see the Supporting Information. The kinetic analysis employed the stretched exponential approach by Wildman and Siebrand.[13] Equation 1 assumes a continuum of reaction rates, implemented by the use of a dispersion coefficient β.

$$I = I_0 \cdot \exp(-(k \cdot t)^{\beta}) + c \qquad \text{with } 0 < \beta < 1 \tag{1}$$

Computational details

Geometry optimizations and vibrational frequency calculations were performed using the BLYP functional (Becke exchange[14] combined with the Lee-Yang-Parr correlation functional[15]) and the Grimme D3 dispersion correction[16] together with the Pople 6–311G** basis sets[17] as implemented in Gaussian 09.[18] In order to reduce computational costs within the Coulomb part, density fitting (DF) with automated generation of auxiliary basis sets was applied.[19] Throughout, tight convergence criteria were employed. The Synchronous Transit-Guided Quasi-Newton (STQN) method[20] with the QST3 algorithm was utilized in order to optimize the geometries of first-order transition states (TS). Tunneling rates were calculated using combination of transition state theory (TST) and semiclassical Wentzel-Kramers-Brillouin (WKB) theory as implemented in the Polyrate program.[21] The calculations were carried out using the Gaussrate[22] interface of Polyrate to the Gaussian 09 package employing the level of theory detailed above. The transmission coefficients for tunneling were calculated with the small-curvature tunneling (SCT) method.[23] The tabulated TST/SCT data refer to conventional (non-variational TST) plus SCT corrections. Due to numerical issues arising at very low temperatures, calculations were carried out at 20 K, where classical barrier passage still is completely suppressed for all processes under consideration.

Acknowledgements

This work was supported by the Deutsche Forschungsgemeinschaft (DFG, German Research Foundation) under Germany's Excellence Strategy – EXC-2033 – Projektnummer 390677874 RESOLV and the Research Training Group "Confinement-controlled Chemistry" (Grant GRK2376/331085229). Open Access funding enabled and organized by Projekt DEAL.

Conflict of Interest

The authors declare no conflict of interest.

Keywords: carbenes · ENDOR spectroscopy · hydrogen transfer · matrix isolation · tunneling

[1] a) M. J. Vetticatt, D. A. Singleton, *Org. Lett.* **2012**, *14*, 2370–2373; b) C. Doubleday, R. Armas, D. Walker, C. V. Cosgriff, E. M. Greer, *Angew. Chem. Int. Ed.* **2017**, *56*, 13099–13102; *Angew. Chem.* **2017**, *129*, 13279–13282; c) P. R. Schreiner, *Trends Chem.* **2020**, *2*, 980–989; d) *Tunnelling in Molecules: Nuclear Quantum Effects from Bio to Physical Chemistry* (Eds: J. Kästner, S. Kozuch), The Royal Society of Chemistry, **2021**.

[2] a) P. R. Schreiner, H. P. Reisenauer, D. Ley, D. Gerbig, C.-H. Wu, W. D. Allen, *Science* **2011**, *332*, 1300–1303; b) A. Kohen, R. Cannio, S. Bartolucci, J. P. Klinman, *Nature* **1999**, *399*, 496–499; c) S. Henkel, Y. a. Huynh, P. Neuhaus, M. Winkler, W. Sander, *J. Am. Chem. Soc.* **2012**, *134*, 13204–13207; d) J. P. Layfield, S. Hammes-Schiffer, *Chem. Rev.* **2014**, *114*, 3466–3494; e) S. Hu, S. C. Sharma, A. D. Scouras, A. V. Soudackov, C. A. M. Carr, S. Hammes-Schiffer, T. Alber, J. P. Klinman, *J. Am. Chem. Soc.* **2014**, *136*, 8157–8160; f) C. M. Nunes, S. N. Knezz, I. Reva, R. Fausto, R. J. McMahon, *J. Am. Chem. Soc.* **2016**, *138*, 15287–15290.

[3] a) O. L. Chapman, R. J. McMahon, P. R. West, *J. Am. Chem. Soc.* **1984**, *106*, 7973–7974; b) R. J. McMahon, O. L. Chapman, *J. Am. Chem. Soc.* **1987**, *109*, 683–692.

[4] a) T. Schleif, J. Mieres-Perez, S. Henkel, E. Mendez-Vega, H. Inui, R. J. McMahon, W. Sander, *J. Org. Chem.* **2019**, *84*, 16013–16018; b) J. P. L. Roque, C. M. Nunes, L. P. Viegas, N. A. M. Pereira, T. M. V. D. Pinho e Melo, P. R. Schreiner, R. Fausto, *J. Am. Chem. Soc.* **2021**, *143*, 8266–8271.

[5] a) A. Mardyukov, H. Quanz, P. R. Schreiner, *Nat. Chem.* **2017**, *9*, 71–76; b) A. K. Eckhardt, F. R. Erb, P. R. Schreiner, *Chem. Sci.* **2019**, *10*, 802–808.

[6] P. S. Zuev, R. S. Sheridan, T. V. Albu, D. G. Truhlar, D. A. Hrovat, W. T. Borden, *Science* **2003**, *299*, 867–870.

[7] P. Costa, T. Lohmiller, I. Trosien, A. Savitsky, W. Lubitz, M. Fernandez-Oliva, E. Sanchez-Garcia, W. Sander, *J. Am. Chem. Soc.* **2016**, *138*, 1622–1629.

[8] a) P. R. Schreiner, J. P. Wagner, H. P. Reisenauer, D. Gerbig, D. Ley, J. Sarka, A. G. Császár, A. Vaughn, W. D. Allen, *J. Am. Chem. Soc.* **2015**, *137*, 7828–7834; b) T. Schleif, J. Mieres-Perez, S. Henkel, M. Ertelt, W. T. Borden, W. Sander, *Angew. Chem. Int. Ed.* **2017**, *56*, 10746–10749; *Angew. Chem.* **2017**, *129*, 10886–10889; c) J. P. Wagner, H. P. Reisenauer, V. Hirvonen, C.-H. Wu, J. L. Tyberg, W. D. Allen, P. R. Schreiner, *Chem. Commun.* **2016**, *52*, 7858–7861.

[9] a) M. Oki, *Acc. Chem. Res.* **1984**, *17*, 154–159; b) J. I. Seeman, *Chem. Rev.* **1983**, *83*, 83–134.

[10] H.-H. Limbach, J. Miguel Lopez, A. Kohen, *Philos. Trans. R. Soc. B* **2006**, *361*, 1399–1415.

[11] I. R. Dunkin, *Matrix Isolation Techniques: A Practical Approach*, Oxford University Press, Oxford, New York, **1998**.

[12] E. Reijerse, F. Lendzian, R. Isaacson, W. Lubitz, *J. Magn. Reson.* **2012**, *214*, 237–243.

[13] W. Siebrand, T. A. Wildman, *Acc. Chem. Res.* **1986**, *19*, 238–243.

[14] A. D. Becke, *Phys. Rev. A* **1988**, *38*, 3098–3100.

[15] C. Lee, W. Yang, R. G. Parr, *Phys. Rev. B* **1988**, *37*, 785–789.

[16] S. Grimme, J. Antony, S. Ehrlich, H. Krieg, *J. Chem. Phys.* **2010**, *132*, 154104.

[17] R. Krishnan, J. S. Binkley, R. Seeger, J. A. Pople, *J. Chem. Phys.* **1980**, *72*, 650–654.

[18] M. J. Frisch, G. W. Trucks, H. B. Schlegel, G. E. Scuseria, M. A. Robb, J. R. Cheeseman, G. Scalmani, V. Barone, B. Mennucci, G. A. Petersson, H. Nakatsuji, M. Caricato, X. Li, H. P. Hratchian, A. F. Izmaylov, J. Bloino, G. Zheng, J. L. Sonnenberg, M. Hada, M. Ehara, K. Toyota, R. Fukuda, J. Hasegawa, M. Ishida, T. Nakajima, Y. Honda, O. Kitao, H. Nakai, T. Vreven, J. A. Montgomery, J. E. Peralta, F. Ogliaro, M. Bearpark, J. J. Heyd, E. Brothers, K. N. Kudin, V. N. Staroverov, R. Kobayashi, J. Normand, K. Raghavachari, A. Rendell, J. C. Burant, S. S. Iyengar, J. Tomasi, M. Cossi, N. Rega, J. M. Millam, M. Klene, J. E. Knox, J. B. Cross, V. Bakken, C. Adamo, J. Jaramillo, R. Gomperts, R. E. Stratmann, O. Yazyev, A. J. Austin, R. Cammi, C. Pomelli, J. W. Ochterski, R. L. Martin, K. Morokuma, V. G. Zakrzewski, G. A. Voth, P. Salvador, J. J. Dannenberg, S. Dapprich, A. D. Daniels, O. Farkas, J. B. Foresman, J. V. Ortiz, J. Cioslowski, D. J. Fox, *Gaussian 09, Revision D.01*, Gaussian, Inc., Wallingford, CT, **2009**.

[19] a) B. I. Dunlap, *J. Chem. Phys.* **1983**, *78*, 3140–3142; b) B. I. Dunlap, *J. Mol. Struct.: THEOCHEM* **2000**, *529*, 37–40.

[20] C. Peng, H. Bernhard Schlegel, *Isr. J. Chem.* **1993**, *33*, 449–454.

[21] J. Zheng, J. L. Bao, R. Meana-Pañeda, S. Zhang, B. J. Lynch, J. C. Corchado, Y.-Y. Chuang, P. L. Fast, W.-P. Hu, Y.-P. Liu, G. C. Lynch, K. A. Nguyen, C. F. Jackels, A. Fernandez Ramos, B. A. Ellingson, V. S. Melissas, J. Villà, I. Rossi, E. L. Coitiño, T. V. A. J. Pu, A. Ratkiewicz, R. Steckler, B. C. Garrett, A. D. Isaacson, D. G. Truhlar, *POLYRATE17*, University of Minnesota, Minneapolis, MN, **2017**.

[22] J. Zheng, J. L. Bao, S. Zhang, J. C. Corchado, R. Meana-Pañeda, Y.-Y. Chuang, E. L. Coitiño, B. A. Ellingson, D. G. Truhlar, *Gaussrate 17*, University of Minnesota, Minneapolis, MN, **2017**.

[23] a) D.-h. Lu, T. N. Truong, V. S. Melissas, G. C. Lynch, Y.-P. Liu, B. C. Garrett, R. Steckler, A. D. Isaacson, S. N. Rai, G. C. Hancock, J. G. Lauderdale, T. Joseph, D. G. Truhlar, *Comput. Phys. Commun.* **1992**, *71*, 235–262; b) Y. P. Liu, G. C. Lynch, T. N. Truong, D. H. Lu, D. G. Truhlar, B. C. Garrett, *J. Am. Chem. Soc.* **1993**, *115*, 2408–2415.

Manuscript received: June 7, 2021
Accepted manuscript online: August 4, 2021
Version of record online: September 12, 2021

